

DFTT 39/95

DTP/95/56

June 1995

Finite width and irreducible background effects to $t\bar{t}$ production at $\gamma\gamma$ Next Linear Colliders¹

Stefano Moretti²

*Dipartimento di Fisica Teorica, Università di Torino,
and I.N.F.N., Sezione di Torino,
Via Pietro Giuria 1, 10125 Torino, Italy.*

*Department of Physics, University of Durham,
South Road, Durham DH1 3LE, United Kingdom.*

PACS number(s): 13.65.+i, 14.70.Bh, 13.60.Fz, 14.65.Ha.

Abstract

We study the complete process $\gamma\gamma \rightarrow b\bar{b}W^+W^-$ using exact matrix element computations at tree-level, at a $\sqrt{s} = 500$ GeV e^+e^- linear collider of the next generation. Incoming photons produced via back-scattering of laser light are considered. Sizable effects due to the finite width of the top quark as well as to the irreducible background to $t\bar{t}$ production and decay are predicted.

¹Work supported in part by Ministero dell' Università e della Ricerca Scientifica.

E-mails: Moretti@to.infn.it; Stefano.Moretti@durham.ac.uk.

²Address after September 1995: Cavendish Laboratory, University of Cambridge, Madingley Road, Cambridge, CB3 0HE, U.K.

1. Introduction

In the past few years the importance of studying the $t\bar{t}$ threshold region through $\gamma\gamma$ collisions at an e^+e^- Next Linear Collider (NLC) has clearly come out.

The option of high energy photon-photon interactions at a NLC would principally make use of well focused high energy γ 's produced through back-scattering of laser light from the electron/positron beams [1], even though photonic interactions can take place also via beamsstrahlung [2], as well as via conventional bremsstrahlung. Photons can interact through their quark and gluon constituents ('resolved' photons). However, in the case of $t\bar{t}$ production the resolved photon rates are fairly small: this mainly depends on the steeply falling parton distributions inside the photon itself³.

It has been established by recent measurements that $m_t \gtrsim 160$ GeV [3], therefore the top lifetime is expected to be shorter than the typical time-scale of strong interactions (i.e., $\Gamma_t > \Lambda_{QCD}$). In this case, within the Standard Model (\mathcal{SM}), top quarks should decay to bW pairs before toponium formation can occur. This has two important consequences. On the one hand, we do not expect any narrow QCD resonance around the energy $2m_t$ (as for $c\bar{c}$ and $b\bar{b}$ bound states) and, on the other hand, the large top width ($\Gamma_t \gtrsim 1.5$ GeV) introduces a natural infrared cut-off, such that it is possible to study all the threshold region within the context of perturbation theory [4, 5]. In fact, the strong running coupling constant α_s occurs at the scale $Q^2 \approx m_t \sqrt{\Gamma_t^2 + E^2}$ (with $E = \sqrt{s} - 2m_t$), which never gets small.

The main possibilities offered by the $\gamma\gamma \rightarrow t\bar{t}$ process are the following. First, by measuring the shape and the position of the $t\bar{t}$ threshold one could determine both m_t and α_s [6, 7]. Second, one can measure Γ_t (thereby checking the value of the Cabibbo-Kobayashi-Maskawa term $|V_{tb}|$) if an energy resolution of $\Delta E_{\gamma\gamma} \lesssim 1$ GeV can be achieved [8]. Third, with $\gtrsim 95\%$ polarized γ beams of opposite helicities (which strongly suppress the dominant s -wave) it is possible to directly study $t\bar{t}$ -production in p -wave, whereas for e^+e^- collisions p -wave production can be probed only by its interference with the s -wave one [6, 9]. Finally, by linearly polarized photon beams one is able to determine the top quark polarization, thus providing a powerful tool to study final QCD interactions and to precisely measure α_s [10]. The cross section for $\gamma\gamma \rightarrow t\bar{t}$ is comparable to the one of $e^+e^- \rightarrow t\bar{t}$, becoming even larger for $\sqrt{s} \gtrsim 500$

³In our analysis we deal with back-scattered photons and with 'direct' $\gamma\gamma$ interactions only.

GeV.

It is the aim of this brief report to add further elements to the argument, by computing all the irreducible background in $\gamma\gamma \rightarrow b\bar{b}W^+W^-$ events, as well as by treating finite top width effects in the appropriate way, without resorting neither to the off-shell production \times Breit-Wigner decay approach nor to the Narrow Width Approximation (NWA), while keeping into account all spin and energy correlations between the two top decays. We do not include here the QCD (and QED) Coulomb-like interactions between the two top quarks at threshold (they lead to an enhancement of the cross section). We do not do that for two reasons. First, the large top mass allow us to conclude that the resonant structures in $t\bar{t}$ production are largely smeared out and do not show up dramatically in the excitation curve. Second, since the Coulomb corrections to $t\bar{t}$ production are part of the higher order corrections and the non resonant background is evaluated here at tree-level, we have ignored them for consistency. For the same reason we have not computed gluon bremsstrahlung radiative corrections.

This study resembles the corresponding analysis done for $e^+e^- \rightarrow b\bar{b}W^+W^-$ in ref. [12]. We turned to the $\gamma\gamma$ case since we expect the finite width effects of the top to be largely independent of the production mechanism, therefore they should remain important in this context as well. In addition, since the process $\gamma\gamma \rightarrow b\bar{b}W^+W^-$ involves 114 Feynman diagrams at tree-level, compared to the 61 occurring in $e^+e^- \rightarrow b\bar{b}W^+W^-$, we expect the irreducible background to be quantitatively even more important here. Finally, the fact that the incoming photons do not have a fixed energy and momentum, but these are spread according to the back-scattering spectrum, introduces a smearing in the differential distributions, which tends to wash out effects typical of $t\bar{t}$ resonant production. Similar effects occur also in connection with, e.g., the Initial State Radiation (ISR) in e^+e^- annihilations. We expect the signal to be sensitive to all of these more than the non resonant $\gamma\gamma \rightarrow b\bar{b}W^+W^-$ production.

The paper is structured as follows. In sect. 2 we give details of the calculations. In sect. 3 we describe and comment on the results we obtained. A brief summary including our conclusions will be given in sect. 4.

2. Computation

The process $\gamma\gamma \rightarrow b\bar{b}W^+W^-$ is described at tree-level by 114 Feynman graphs. Their structure is very rich, including (apart from Higgs self interactions) all the types of \mathcal{SM} couplings at tree-level⁴. Seven subsets of the graphs are displayed in fig. 1. Out of the original 114 diagrams, we tried to separate the most topologically different ones. We recognised the following structures, of diagrams involving: a) four vertices Vff' , where $V = \gamma, Z$ or W , and $ff' = bb$ or bt : 12 graphs; b) three vertices Vff' , and one W^+W^-V' , where $V = \gamma, Z$, or W , $V' = \gamma$ or Z , and $ff' = bb$ or bt : 24 graphs; c) two vertices Vff' , and two connected W^+W^-V' , where $V = \gamma, Z$, or W , $V' = \gamma$ or Z , and $ff' = bb$ or bt : 20 graphs; d) two vertices Vff' , and two disconnected W^+W^-V' , where $V = W$, $V' = \gamma$, and $ff' = bt$: 2 graphs; e) one vertex Vff' , and three (connected) W^+W^-V' , where $V = V' = \gamma$ or Z , and $ff' = bb$: 12 graphs; f) two vertices Vff' , and one $W^+W^-\gamma V'$, where $V = \gamma, Z$, or W , $V' = \gamma$ or Z , and $ff' = bb$ or bt : 10 graphs; g) one vertex Vff' , one $W^+W^-\gamma$, and one $W^+W^-\gamma V'$, where $V = V' = \gamma$ or Z , and $ff' = bb$: 12 graphs.

All the necessary diagrams can be obtained by the topologies of fig. 1 by properly labeling both the internal and external lines following the indications given in a–g. In addition, to get the contributions involving internal Higgs lines (22 graphs) one has to replace for any virtual $V = \gamma, Z$ the H , apart from the case of quartic couplings $W^+W^-\gamma V$. The different sets in a–g correspond to different structures of the **FORT**RAN routines too.

The matrix element for $\gamma\gamma \rightarrow b\bar{b}W^+W^-$ has been computed with the help of MadGraph/HELAS [13]. In order to keep the interplay between the various resonances which appear in the integration domains of the final state $b\bar{b}W^+W^-$, when all tree-level contributions are kept into account, under control, we have adopted the technique of splitting the Feynman amplitude squared into a sum of different (non-gauge-invariant) terms, each of which has been integrated according to its resonant structure with an appropriate choice of integration variables and phase space. The gauge invariance is recovered by summing at the end the integrated contributions of the above terms, both in the total and the differential rates. This procedure has been carefully described elsewhere [14], so we do not enter here into details. The multi-

⁴Therefore they also constitute a useful tool to test the model itself.

dimensional integrations over the phase space have been performed numerically using VEGAS [15].

The following values of the parameters have been adopted: $M_Z = 91.1$ GeV, $\Gamma_Z = 2.5$ GeV, $M_W \equiv M_Z \cos(\theta_W) \approx 80$ GeV, $\Gamma_W = 2.2$ GeV, and $\sin^2(\theta_W) = 0.23$. For the fermions: $m_b = 5$ GeV and $m_t = 175$ and 200 GeV, according to the values announced by CDF and D0. The top width Γ_t has been computed at tree-level, for coherence⁵. In order to get rid of complications due to virtual Higgs contributions we have deliberately decided to set M_H equal to a value which strongly suppresses them (at $\sqrt{s} = 500$ GeV, e.g., $M_H = 700$ GeV). Also for the Higgs width we have adopted the expression at tree-level. The electromagnetic coupling constant has been set equal to $1/128$. We have carried out our analysis at the standard energy $\sqrt{s} = 500$ GeV. Finally, we have not implemented the effects due to the finite width of the final state W 's: we are confident, however, that taking them into account would not affect our conclusions.

3. Results

The results we obtained are presented throughout tab. I and figs. 2–4. In the following we will adopt the notations ‘NWA’, ‘Production & decay’, ‘All diagrams’, to indicate the three processes $\gamma\gamma \rightarrow t\bar{t} \rightarrow b\bar{b}W^+W^-$, $\gamma\gamma \rightarrow t^*\bar{t}^* \rightarrow b\bar{b}W^+W^-$ and $\gamma\gamma \rightarrow b\bar{b}W^+W^-$, respectively. In the first reaction, the top quarks are produced on-shell and subsequently decay to bW pairs. In order to achieve this we have kept into the computations only the two graphs of ‘type a’ in which both the photons couple to the top line, and we have re-written the top propagator as

$$\frac{\not{p} + m_t}{p^2 - m_t^2 + im_t\Gamma} \left(\frac{\Gamma}{\Gamma_t} \right)^{1/2}, \quad (1)$$

then we have taken $\Gamma \rightarrow 0$. In this limit, the square of eq. (1) produces a $\delta(p^2 - m_t^2)$ (i.e., giving on-shell $t\bar{t}$ production). Numerically, we used $\Gamma = 10^{-5}$, which produces results in very good agreement with those from the two-to-two body reaction $\gamma\gamma \rightarrow t\bar{t}$. In the second process, the top quarks are produced also off-shell by setting $\Gamma = \Gamma_t$ with Γ_t finite (so the standard expression from the propagator is recovered), and by using again the two above diagrams only. In the third case, all the diagrams entering at

⁵This is needed in fact to recover the $\gamma\gamma \rightarrow t\bar{t}$ cross section in NWA (see later on).

tree-level into the process $\gamma\gamma \rightarrow b\bar{b}W^+W^-$ are computed (graphs a+b+c+d+e+f+g), with the same convention as in $\gamma\gamma \rightarrow t^*\bar{t}^* \rightarrow b\bar{b}W^+W^-$ for the top propagators (apart from the case of t -channel propagators, which have no imaginary part).

Tab. I shows that the irreducible background to $t^{(*)}\bar{t}^{(*)}$ production and decay is not negligible, since it gives an additional contribution which is $\approx 21(500)\%$ for $m_t = 175(200)$ GeV, with respect the on-shell $t\bar{t}$ production: much(enormously) larger than in the case of e^+e^- initiated top pair production (see ref. [12]). The difference between the case ‘NWA’ and ‘Production & decay’ are of $\approx 3(20)\%$, and the rates are larger in the first(second) case. This reflects the fact that, for $m_t = 175$ GeV, increasing the top width in the square of the propagator (1) reduces the total cross section more than phase space reduction by requiring two on-shell top quarks (see also tab. II in ref. [12]), whereas if $m_t = 200$ GeV the situation is the other way round.

In order to understand the large difference in the total cross sections for the two different values of m_t , we notice that the peak in the energy distribution of a backscattered photon is roughly at $\approx 0.8 \times (\sqrt{s}/2) \approx 200$ GeV. The fact that the cross section for $m_t = 200$ GeV is much smaller than the one for $m_t = 175$ GeV indicates that the quantity $E = \sqrt{s} - 2m_t$ is negative most of the times (i.e., $t\bar{t}$ production below threshold occurs).

Since we expect Γ_t to influence the kinematics of the top decay products b and W , we studied in fig. 2 the dependence of the cross sections, e.g., on the momentum of the W , for $\gamma\gamma \rightarrow t\bar{t} \rightarrow b\bar{b}W^+W^-$, $\gamma\gamma \rightarrow t^*\bar{t}^* \rightarrow b\bar{b}W^+W^-$ and $\gamma\gamma \rightarrow b\bar{b}W^+W^-$. Whereas, in the case of e^+e^- annihilation, the fact that the system e^+e^- has a fixed energy (apart from beamsstrahlung and ISR effects), equal to \sqrt{s} , allows to opportunely tune the collider energy in order to study $t\bar{t}$ production at few GeV above threshold and to deduce the top mass from the p_W spectrum [16], in photon-photon collision this is quite problematic. In fact, the invariant mass of the $\gamma\gamma$ system is not fixed but follows a luminosity distribution. Therefore, no clear edge appears in the p_W distribution in the case of NWA. Also, contrary to the case of e^+e^- top production, no systematic difference in the shape of the curves for $\gamma\gamma \rightarrow t\bar{t} \rightarrow b\bar{b}W^+W^-$, $\gamma\gamma \rightarrow t^*\bar{t}^* \rightarrow b\bar{b}W^+W^-$ and $\gamma\gamma \rightarrow b\bar{b}W^+W^-$ occurs (see fig. 2 in ref. [12]).

However, this variable represents a good choice for studying the effects due to the increase of the top width, connected with the possible existence of new physics

beyond the \mathcal{SM} . In fact, fig. 3 shows the strong sensitivity of p_W on Γ_t , in the case this latter is increased by a factor of 1.25 and 1.5. The integrated cross sections give 50.16(9.32) and 34.83(8.12) fb, respectively, for the two usual values of the top mass, to be compared with the values in the third column of tab. I. Here, the complete process $\gamma\gamma \rightarrow b\bar{b}W^+W^-$ is considered.

In order to get rid of the irreducible background, a natural procedure appears to be cutting around the narrow top peak in the invariant mass of the bW system ($\Gamma_t \lesssim 2.5$ GeV for $m_t \lesssim 200$ GeV). However, once one has reconstructed the W from its decay products (leptons or hadrons) there is still an ambiguity in assigning the third jet, since this can be produced either by the ‘right’ b (the one coming in association with the tagged W in the same top decay) or by the ‘wrong’ b (the one coming from the other top decay). Therefore, one usually constructs two combinations bW , with only one peaking at m_t . A way of avoiding this could be to recognise the charge of the parton from which the jets originate (e.g., by the ‘jet charge’ method or by tagging the lepton from the decaying b). However, this is unlikely to give high efficiencies, since in order to enhance the signal rates the other W is usually tagged by its hadronic decays, therefore, one ends up dealing with at least 4 jets in the final state.

In fig. 4 we show the invariant mass of the right and wrong bW combinations, plotted in 10 GeV bins. For example, the areas in the range $|M_{bW} - m_t| \leq 10$ GeV are $\approx 60(4.81)$ and $\approx 6(0.88)$ fb, for $m_t = 175(200)$ GeV, respectively. Therefore the contamination of unwanted wrong bW combinations in peaking up events around the top mass is $\approx 10(18)\%$, depending on the top mass itself. These percentages roughly represent the size of the errors in the analyses which select the candidate $t\bar{t}$ sample by cutting in the reconstructed bW invariant mass. At the same time, the two distributions in fig. 3 sum up to just one, with the effect of making the top peak broader and the eventual determination of Γ_t from this spectrum quite problematic. This effect is more important here than in e^+e^- collisions.

4. Summary and conclusions

We have studied differential and integrated rates for the processes $\gamma\gamma \rightarrow t\bar{t} \rightarrow b\bar{b}W^+W^-$, $\gamma\gamma \rightarrow t^*\bar{t}^* \rightarrow b\bar{b}W^+W^-$ and $\gamma\gamma \rightarrow b\bar{b}W^+W^-$, by incoming photons generated via Compton back-scattering of laser light. We used exact matrix element

calculations at tree-level. In the first case only the on-shell $t\bar{t}$ -production is computed, in the second reaction also off-shell and finite width effects of the top are included, whereas in the third process all the gauge invariant set of Feynman diagrams is considered and no approximation is adopted. This allowed us to estimate that the irreducible background in $b\bar{b}W^+W^-$ final states to the process $\gamma\gamma \rightarrow t\bar{t}$ at a NLC with $\sqrt{s} = 500$ GeV increases the integrated $t\bar{t}$ signal rates by $\approx 21\%$ (a factor of 5), if $m_t = 175(200)$ GeV. At $\sqrt{s} = 500$ GeV, the two values $m_t = 175$ and 200 GeV correspond to the two opposite cases in which $t\bar{t}$ -pairs are produced above and below the threshold $2m_t$, respectively. As for a NLC operating in the $\gamma\gamma$ -mode the Center-of-Mass (CM) energy of the photons is not fixed but follows a luminosity distribution, both of these are realistic conditions. Therefore, this clearly shows how both an excellent determination of m_t and a careful tuning of the energy \sqrt{s} of the e^+e^- system are needed, in order to control non resonant $b\bar{b}W^+W^-$ events and to study in detail the $t\bar{t}$ -threshold via $\gamma\gamma$ -collisions.

The top finite width effects have been studied by comparing the on-shell $t\bar{t}$ production and decay in NWA with the off-shell one. Here, differences vary from 3 to 20%, depending on the top mass. Moreover, if the top width turns out to be larger than the \mathcal{SM} one, due to possible new physics, sizable effects are expected.

Before drawing definite conclusions these results should be folded with a realistic simulation including the expected performances of the detectors of a NLC, and studied depending on the adopted experimental strategies. High order corrections (Coulomb singularities, gluon and photon radiative corrections, ISR, etc ...) should be properly included as well. However, our predictions seem to indicate that effects due to the unavoidable presence of the irreducible background and to the finite width of the top should be included in the phenomenological analyses.

Acknowledgements

We are grateful to V.A. Khoze for useful comments and for reading the manuscript.

References

- [1] V. Telnov, *Nucl. Instrum. Methods* **A294** (1990) 72;
I. Ginzburg, G. Kotkin, V. Serbo and V. Telnov, *Nucl. Instrum. Methods* **A205** (1983) 47, **A219** (1984) 5.
- [2] R.J. Noble, *Nucl. Instrum. Methods* **A256** (1976) 427.
- [3] CDF Coll., *preprint* FERMILAB-PUB-94/022-E, CDF/PUB/TOP/PUBLIC /3040, March 1995;
D0 Coll., *preprint* FERMILAB-PUB-95-028-E, March 1995.
- [4] V.S. Fadin and V.A. Khoze, *JETP Lett.* **46** (1987) 525; *Sov. J. Nucl. Phys.* **53** (1988) 692.
- [5] I.I. Bigi, Y. Dokshitzer, V.A. Khoze, J.H. Kühn and P.M. Zerwas, *Phys. Lett.* **B181** (1986) 157.
- [6] E. Boos *et al.*, *Z. Phys.* **C56** (1992) 487;
J.H. Kühn, E. Mirkes, and J. Steegborn, *Z. Phys.* **C57** (1993) 615;
O.J.P. Eboli, M.C. Gonzalez-Garcia and F. Halzen, *Phys. Rev.* **D47** (1993) 1889.
- [7] I.I. Bigi, F. Gabbiani and V.A. Khoze, *Nucl. Phys.* **B406** (1993) 3.
- [8] M.S. Chanowitz, *preprint* LBL-35776, June 1994, to be published in the Proceedings of the Workshop on Gamma-Gamma Colliders, Berkeley, CA, 28-31 March 1994.
- [9] H. Murayama and Y. Sumino, *Phys. Rev.* **D47** (1993) 82;
K. Fujii, T. Matsui and Y. Sumino, *Phys. Rev.* **D50** (1994) 4341.
- [10] V.S. Fadin, V.A. Khoze and M.I. Kotskii, *Z. Phys.* **C64** (1994) 45;
W. Benreuther, J.P. Ma and B.H.J. McKellar, *preprint* UM-P-94-25, OZ-94-12, PITHA-94-17, April 1994.
- [11] F. Halzen, C.S. Kim and M.L. Stong, *Phys. Lett.* **B274** (1992) 489.
- [12] A. Ballestrero, E. Maina and S. Moretti, *Phys. Lett.* **B333** (1994) 434.
- [13] T. Stelzer and W.F. Long, *Comp. Phys. Comm.* **81** (1994) 357;
E. Murayama, I. Watanabe and K. Hagiwara, HELAS: HELicity Amplitude Subroutines for Feynman Diagram Evaluations, *KEK Report* 91-11, January 1992.

- [14] A. Ballestrero, E. Maina and S. Moretti, *Phys. Lett.* **B335** (1994) 460;
S. Moretti, *U. of Torino preprint* DFTT 69/94, *Durham U. preprint* DTP/95/02,
December 1994.
- [15] G.P. Lepage, *Jour. Comp. Phys.* **27** (1978) 192.
- [16] G. Bagliesi *et al.*, in Proc. of the Workshop “ e^+e^- Collisions at 500 GeV. The
Physics Potential”, Munich, Annecy, Hamburg, 3-4 February 1991, ed. P.M. Zer-
was, DESY pub. 92-123A/B, August 1992; DESY pub. 93-123C, December 1993.

Table Captions

table I Cross sections for the processes $\gamma\gamma \rightarrow t\bar{t} \rightarrow b\bar{b}W^+W^-$ (NWA), $\gamma\gamma \rightarrow t^*\bar{t}^* \rightarrow b\bar{b}W^+W^-$ (Production & decay) and $\gamma\gamma \rightarrow b\bar{b}W^+W^-$ (All diagrams), at $\sqrt{s} = 500$ GeV, for the two values of the top mass $m_t = 175$ and 200 GeV. For the Higgs mass we have taken $M_H = 700$ GeV.

Figure Captions

figure 1 The topologically different subsets of Feynman diagrams contributing at tree-level to $\gamma\gamma \rightarrow b\bar{b}W^+W^-$ (see the text). Continuous lines represent a b or a t , whereas wavy lines refer to a γ , a W , a Z or a H , as appropriate, according to the couplings within the \mathcal{SM} .

figure 2 Differential distribution in the momentum of the W , for the three cases $\gamma\gamma \rightarrow t\bar{t} \rightarrow b\bar{b}W^+W^-$ (continuous lines), $\gamma\gamma \rightarrow t^*\bar{t}^* \rightarrow b\bar{b}W^+W^-$ (dashed lines) and $\gamma\gamma \rightarrow b\bar{b}W^+W^-$ (dotted lines), at $\sqrt{s} = 500$ GeV, for the two values of the top mass $m_t = 175$ and 200 GeV. For the Higgs mass we have taken $M_H = 700$ GeV.

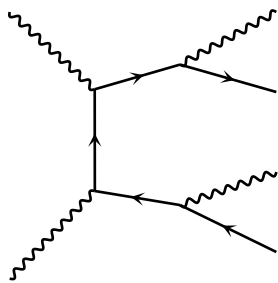
figure 3 Differential distribution in the momentum of the W , in the case $\gamma\gamma \rightarrow b\bar{b}W^+W^-$ only, for the \mathcal{SM} tree-level top width Γ_t (continuous lines), for $1.25 \times \Gamma_t$ (dashed lines) and $1.5 \times \Gamma_t$ (dotted lines), at $\sqrt{s} = 500$ GeV, for the two values of the top mass $m_t = 175$ and 200 GeV. For the Higgs mass we have taken $M_H = 700$ GeV.

figure 4 Differential distribution in the invariant mass of the bW system, in the case $\gamma\gamma \rightarrow b\bar{b}W^+W^-$, for the ‘right’ (continuous lines) and the ‘wrong’ (dashed lines) combinations of b and W (see the text), at $\sqrt{s} = 500$ GeV, for the two values of the top mass $m_t = 175$ and 200 GeV. For the Higgs mass we have taken $M_H = 700$ GeV.

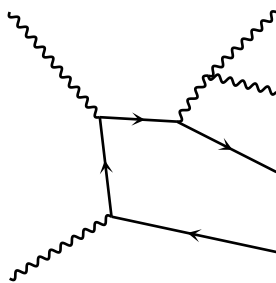
$\sigma(\gamma\gamma \rightarrow X)$ (fb)			
m_t (GeV)	NWA	Production & decay	All diagrams
$\sqrt{s} = 500$ GeV			
175	62.49	60.64	75.90
200	2.03	2.51	10.22
$M_H = 700$ GeV			

Table I

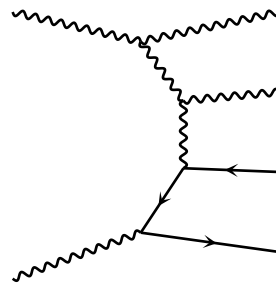
Diagrams by MadGraph



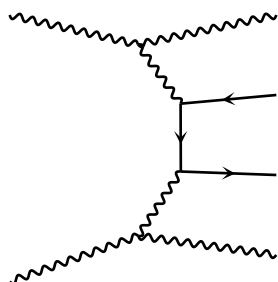
graphs a



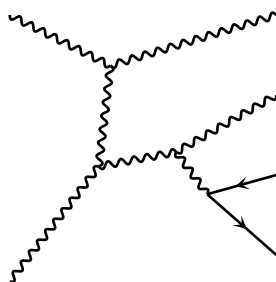
graphs b



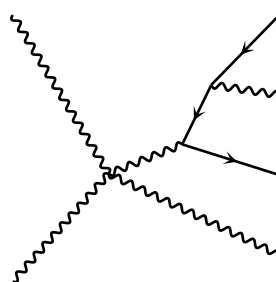
graphs c



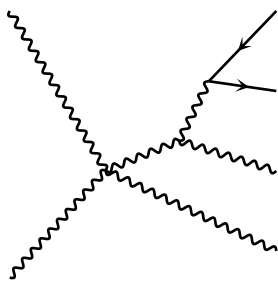
graphs d



graphs e



graphs f



graphs g

Fig. 1

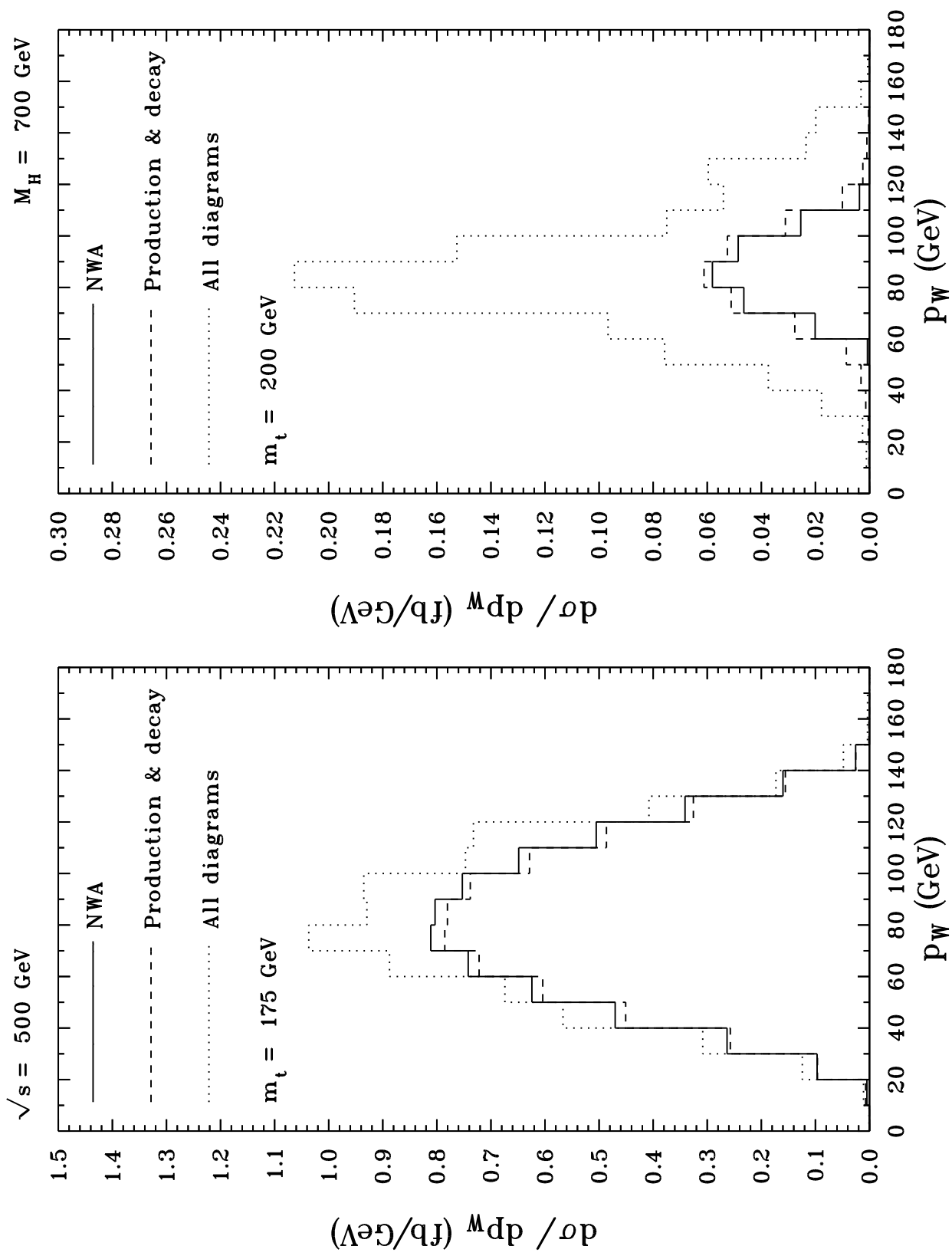


Fig. 2

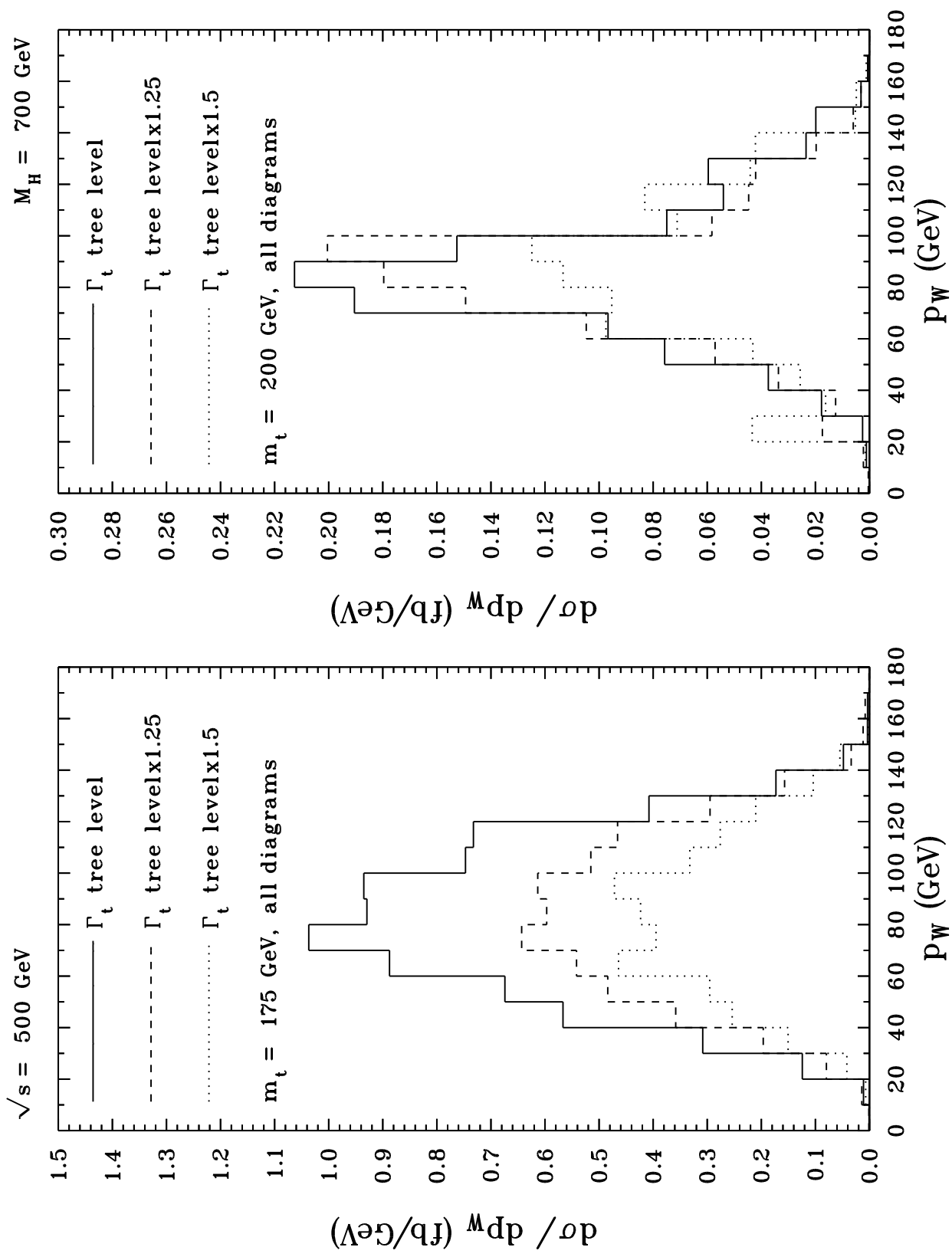


Fig. 3

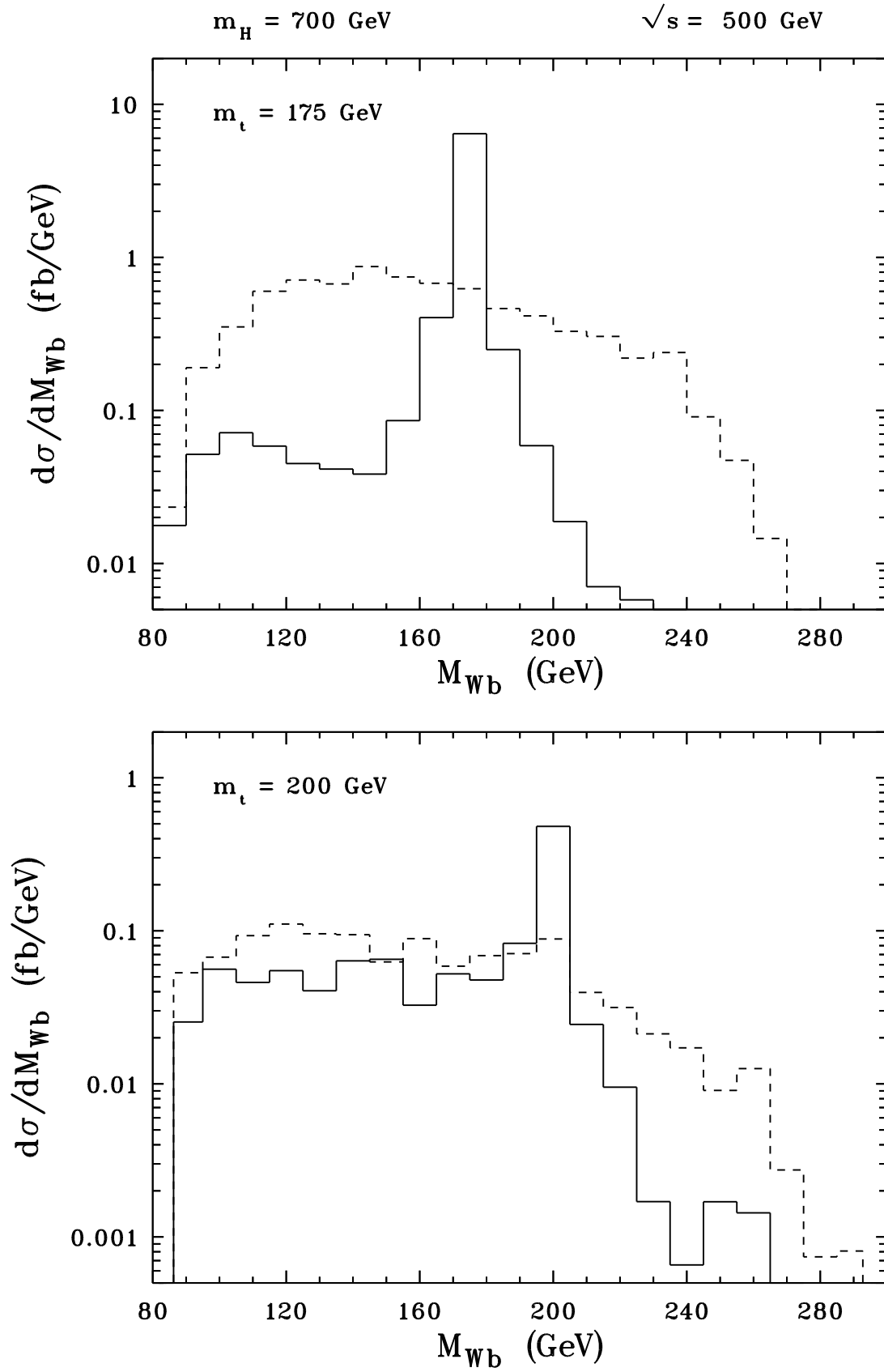


Fig. 4